Proceeding of the IEEE
International Conference on Robotics and Biomimetics
Dali, China, December 2019

Design of A Novel Electromagnetic Actuation System for Actuating Magnetic Capsule Robot

Sishen Yuan[1],Yue Wan[1],Yunxuan Mao[1], Shuang Song[1]*, Max Q.-H. Meng[2], *Fellow, IEEE*

***Abstract*—The active motion control of the magnetic capsule endoscope in the human body is an important guarantee for accurate and complete acquisition of the internal photographs of the gastrointestinal tract. In this paper, we will design a novel electromagnetic actuation system that allows the magnetic capsule endoscope to perform point-to-point movement and fixed point rotation and the potential for this system to enter clinical medicine will be presented thanks to its open structure that can be combined with existing medical equipment, especially the imaging system, for diagnosis and treatment. The system consists of 8 electromagnetic coil modules. In order to optimize space occupancy and energy consumption, we utilize finite element analysis data to parameterize a single electromagnetic coil module. The spatial orientation of electromagnetic coil module is determined according to the geometric parameters of the human stomach and the magnetic field radiation range of electromagnetic coil modules. The mathematical model of the combined magnetic field distribution will be constructed based on the Biot-Savart law, and a simple model of the magnetic capsule endoscope is used to demonstrate the basic functions of this system.**

***Index Terms*—magnetic capsule endoscope, electromagnetic actuation, parametric design.**

I. Introduction

In recent years, magnetic capsule endoscopes having imaging and wireless communication functions in the field of gastrointestinal endoscopes have received extensive attention. This new type of endoscopic device has the advantages of flexibility, small trauma, and no obvious foreign body experience. However, there is still no mature solution for remote operation of small devices inside the human body [1], [2].

The movement form of the capsule robot in the human body can be divided into passive actuation and active actuation. Passive actuation has been widely used in the early development of capsule robots. This type of movement relies on the peristalsis of the gastrointestinal tract to control the displacement of the capsule robot in the body [3]. The incomplete image capture of the $in-vivo$ image caused by the uncontrollability of the position is a prominent shortcoming of this motion mode and cannot be effectively solved temporarily. The main reason for limiting the development of the active actuation mode is that it is difficult to integrate the motion module inside the capsule robot and also to ensure that its overall size is in a few cubic centimeters [4]. However, the simple structure of the magnetic actuation module, which often only needs a kind of hard magnetic material to be embedded inside the robot, can solve this problem well [5]. The use of varying magnetic fields to generate the required force and torque to control the movement of the magnetic capsule robot is the most promising external field control mode due to the quasi-static magnetic field is easy to generate and does not harm the human body [6].

To date, there are two types of mainstream magnetic field generating devices. The first type is that a single permanent magnet generates an ideal magnetic field distribution in space according to a preset trajectory under the operation of a mechanical device. Arthur W. Mahoney et al. used a 6-DOF manipulator to control a single permanent magnet to give the magnetic capsule robot a 3-DOF closed-loop position control and 2-DOF directional open-loop control in the fluid [7]. However, the stability of the movement of the magnetic capsule robot is difficult to guarantee due to the nonlinearity of the magnetic field excited by the permanent magnet. The second type is that multiple stationary electromagnets produce the desired force and torque at the end effector in the workspace after passing in the varying input current vector. One typical electromagnetic actuation system is the generation of the field and the field gradient are separated by design, which is accomplished using combinations of Helmholtz and Maxwell pairs [8], [9]. Chungseon Yu et al. proposed to use the Maxwell and Helmholtz combination coils to generate the uniform magnetic field and the gradient magnetic field to control the direction and force of the magnetic micro-robot [10]. However, the closed structure of the above electromagnetic drive system is difficult to use with other medical functions especially like imaging. Another typical eletromagnetic system consists of an arrangement of stationary eletromagnets and every eletromagnet needs to contribute to both generation of the desired magnetic field and the field gradient [11], [12]. Donghoon Son et al. proposed an open design framework with nine eletromagnets all placed below the workspace. The configuration of the coil model is optimized to produce a strong gradient in the Z direction [13], [14]. The work of Donghoon Son brings

This work was supported in part by National Key R&D Program of China (2018YFB1307700),in part by National Natural Science Foundation of China (61803123),and in part by the Science and Technology Innovation Committee of Shenzhen(JCYJ20170413110250667).

[1]Sishen Yuan, Yue Wan, Yunxuan Mao, Shuang Song are with School of Mechanical Engineering and Automation, Harbin Institute of Technology(Shenzhen), Shenzhen, China, 518055.

[2]Max Q.-H. Meng is with Department of Electronic Engineering, the Chinese University of Hong Kong, Hong Kong, China, and affiliated with the State Key Laboratory of Robotics and Systems (HIT), Harbin Institute of Technology, China.

*Corresponding author: Shuang Song, mail: songshuang@hit.edu.cn

978-1-7281-6321-5/19//$31.00 ©2019 IEEE

inspiration to the design of this article. The magnetic actuation system with expandable performance, especially the multi-information fusion with the imaging system or the magnetic positioning system, is a necessary condition for entering the clinical experiment.

Fig. 1. The prototype of the magnetic operating system. (a) Top view of the system. (b) Side view of the system.

In this paper, as shown in Fig.1, we will propose a prototype of a novel magnetic actuation system with scalability for the specific medical application of magnetic capsule robots in the body of 3-DOF position control and 2-DOF orientation control. To compensate for the two common defects of the electromagnetic system with large energy consumption (large heat generation) and low magnetic field strength, the parametric design and the spatial configuration design of the coil module have been done. More importantly, we will focus on the feasibility and potential of the magnetic actuation system proposed in this paper to achieve the function of magnetic capsule robot actuation.

Structure of this paper is organized as follow: parametric design and performance verification of magnetic field modules and construction of magnetic operating system will be shown in Section II. Mathematical description of spatial magnetic field distribution and experiments on functional demonstration and verification of the magnetic operating system will be shown in Section III. Finally, summary and conclusion of the paper and description of future work will be drawn in Section IV.

II. SYSTEM DESIGN AND CHARACTERIZATION

A. Design of coil module parameters

The electromagnetic actuation system consists of multiple electromagnetic modules that follow a certain spatial distribution. The radiation intensity of the effective magnetic field of the electromagnetic coil module is often positively correlated with the volume of the electromagnetic coil module, but the number of electromagnetic coil modules is negatively correlated with the volume of the electromagnetic coil module. The appropriate coil size will be studied in the following.

As shown in Fig.2, the coil module is mainly composed of four parts, including a framework, a magnetic core, a coil and a connecting structure. The cross-sectional side length and axial length of the cuboid are used as two research factors to optimize the design of the coil module. An FEM analyzing model is developed for simulating the magnetic field

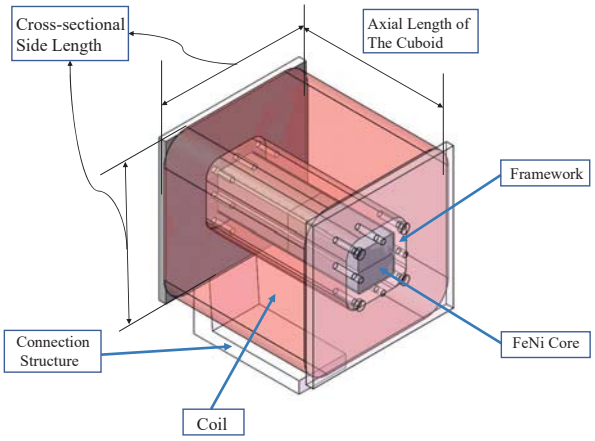

Fig. 2. Conceptual diagram of the coil module.

generation. The FEM model is performed in ANSYS code (ANSYS, Inc., USA). As shown in Fig.3, simulated magnetic field distribution data on two vertical paths is used to evaluate the parametric design of the coil module. The first path is parallel to the axial direction of the coil module and extends from the center point of the end face of the coil module to 200 mm. The second path is perpendicular to the axis of the coil, and is 50 mm parallel to the end face of the coil, and has a total length of 200 mm, which is symmetrical about the axis of the coil.

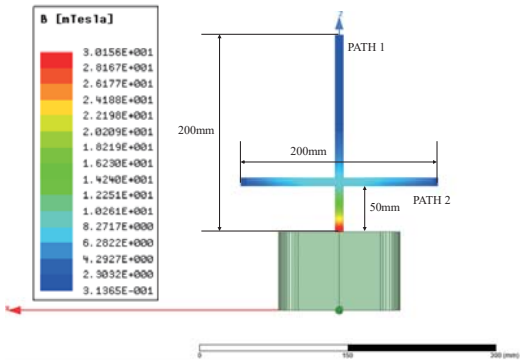

Fig. 3. Two standard paths to characterize the magnetic field distribution of the coil module.

The influence of the axial length of the coil on the magnetic field distribution is first analyzed, as shown in Fig.4 and Fig.5. 80mm, 100mm, 120mm, 140mm, 160mm are five typical coil axial lengths. Fig.4 shows that as the axial length increases, there is only a small gain to the magnetic field on path 1. Fig.5 shows that the magnetic field on path 2 has a larger enhancement effect as the axial length increases. However, when the length is greater than 120 mm, there is no significant difference in magnetic field strength. When the axial length is greater than 120mm, the ratio of the gain of the magnetic field strength to the energy consumption of the coil will be greatly reduced, so the parameter of the axial length of the coil is set to 120mm.

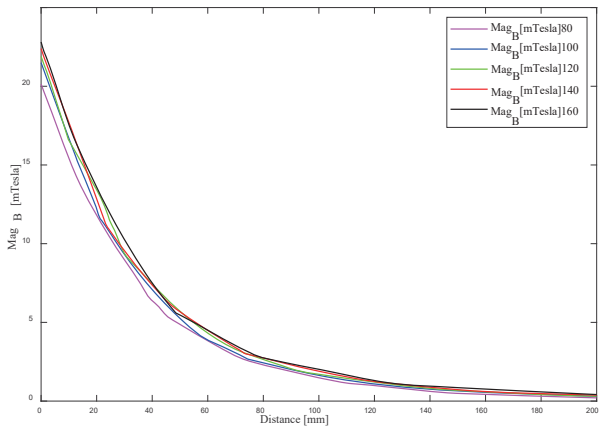

Fig. 4. Influence of axial length of coil on axial magnetic field distribution.

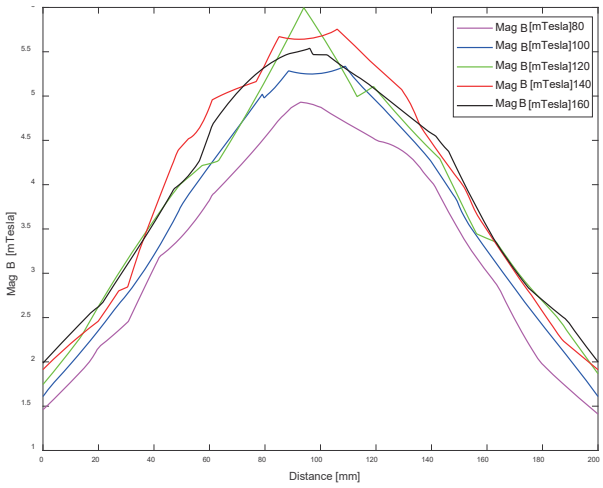

Fig. 5. Influence of axial length of coil on transverse magnetic field distribution.

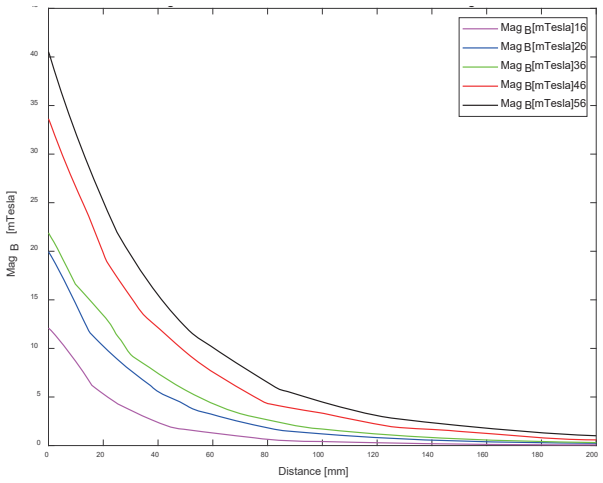

Fig. 6. Influence of the length of the cross section of the coil on the axial magnetic field distribution.

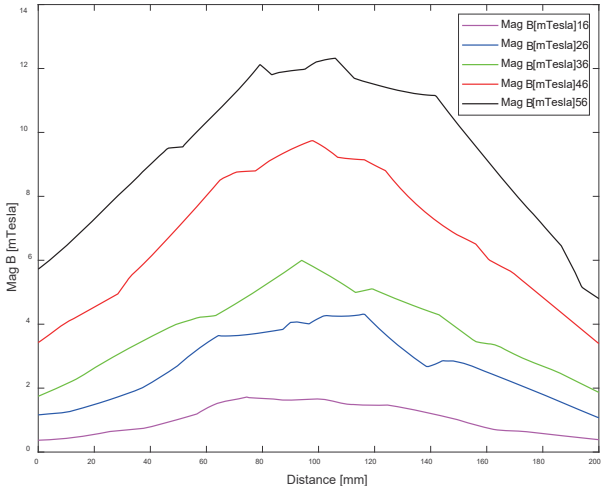

Fig. 7. Influence of the length of the cross section of the coil on the distribution of the transverse magnetic field.

Then the influence of the cross-section length of the coil on the magnetic field distribution is studied, as shown in Fig.6 and Fig.7. 16mm, 26mm, 36mm, 46mm, 56mm are five typical multilayer coil winding thickness values. Results in Fig.6 and Fig.7 indicate that as the length of the cross section of the coil increases, the axial and lateral magnetic field distributions are significantly increased. Although the magnetic field on the two paths increases significantly when the thickness is 46 mm, we mainly avoid the increase in the length of the cross-section leading to the reduction of the volume of the effective radiating magnetic field in the coil module when considering all the factors that determine the length of the cross-section. In this paper, the multilayer coil thickness of 36mm is considered to be a suitable size, and the cross-section side length is 120mm. This parameter will serve the spatial configuration of the coil module.

Finally, as shown in Fig.8, the effect of the soft magnetic core on the magnetic field distribution was investigated. The electromagnet cores are made of H125, which is a FeNi alloy produced by Hengdian Group DMEGC Magnetics CO.,LTD. Its saturation magnetization is on the order of 1500 mT, and the initial permeability is 125 H/m. Fig.9 shows that the magnetic core has an enhancement of at least about 2.3 times the magnetic field strength in the working area. We define the ratio of the magnetic field strength under the assembled iron-nickel soft magnetic core to the magnetic field strength under the non-magnetic core assembly as the gain factor. With the center of the coil end face as the center of the sphere and the radius of 60mm hemisphere, the gain coefficient decreases linearly from 3.65 to 2.3. Outside the hemisphere, the gain coefficient is stable at 2.3. The gain coefficients in the working area will form a correction matrix to accurately represent the magnetic field distribution in the space.

Based on the analysis from these three perspectives, the parameters used for our system design were finally determined(see Table I).

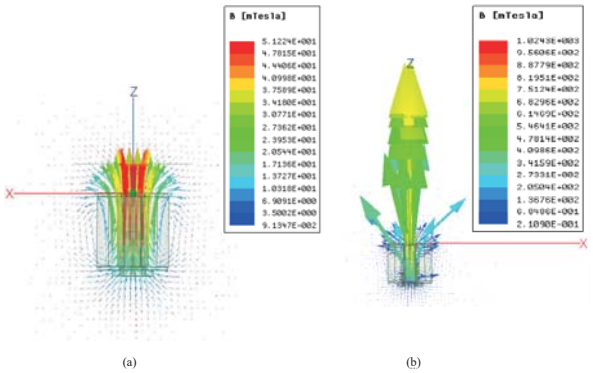

Fig. 8. Effect of iron-nickel soft magnetic core on magnetic field line distribution. (a) Air-core. (b) Iron-nickel soft magnetic core.

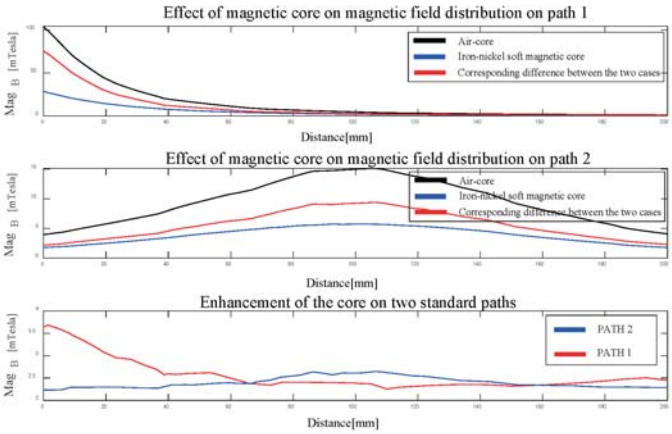

Fig. 9. Effect of iron-nickel soft magnetic core on magnetic field distribution.

After the physical structural parameters of the electromagnetic field are determined, its radiated magnetic field is only related to the input current vector. The experimental measurements show that the simplified model of the magnetic capsule robot requires a magnetic field of at least $3mT$ to obtain an effective torque in a low damping liquid environment. As shown in Fig.10, $3mT$ is used as the critical value to establish the radiation boundary of the coil module based on the simulated data when the coil module flows through the excitation current of $5A$.

TABLE I
PARAMETERS OF EACH ELECTROMAGNETIC COIL

Parameter	Value enameled copper wire	Units
Cross-sectional Side Length	120	mm
Axial Length of The Cuboid	120	mm
Multilayer Coil Thickness	36	mm
Diameter of Coils	2	mm
Number of turns of the coil	900	$\sim$
Coil resistance(R)	1.5	ohm
Shape of cores	Cuboid	-
Material of cores	FeNi	-
Size of cores	$30 \times 30 \times 120$	mm^3

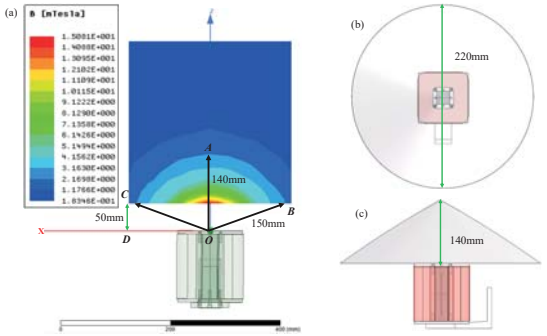

Fig. 10. The radiation boundary of a single coil module. (a) When a current of 5 A is applied, the cross section of the spatial magnetic field distribution is shown. With $3mT$ as the critical value, the physical parameters OA, OB and CD of the effective magnetic field boundary are obtained. (b)(c) The approximately conical region is a visual representation of the effective magnetic field region. Its physical parameters are 220mm and 140mm respectively.

B. Magnetic Manipulation System

The magnetic capsule endoscope performs image acquisition in the stomach mainly depending on the torque applied by the magnetic field to change the shooting angle of the camera lens. It is basically impossible to complete the full scan of the stomach at a single point, so it is necessary to rely on the gradient of the external magnetic field to move the magnetic capsule endoscope to a suitable position to repeat the sweeping operation to capture the picture of the blind spot. Simultaneous control of the torque and force of the magnetic capsule robot requires at least 8 stationary electromagnets [15], but it is difficult to achieve superposition of 8 effective magnetic field radiation regions in the current workspace, as shown in Fig.11, due to the cubic attenuation of the magnetic field magnitude with distance. However, there is no coupling relationship between the torque and force control of the magnetic capsule endoscope based on the analysis above. The literature [16] proved that only three magnets are required to control 3-D field at a point and similarly four magnets are required to control the force on dipole with only magnetic inputs.

Adapting to the physiological structure of the human body, especially the position and shape of the gastrointestinal tract, and optimizing the spatial distribution of the magnetic field module to maximize the area of the effective magnetic field superimposed in the working area are two criteria for our system design. The magnetic manipulation system is built shown in Fig.12which consists of 4 main coil modules in the central area and 4 auxiliary coils arranged at an angle of 45 degrees on the side. Fig.13 and Fig.14 show the visual representation of the spatial distribution of the effective magnetic field of the main coil module and the auxiliary coil module respectively.

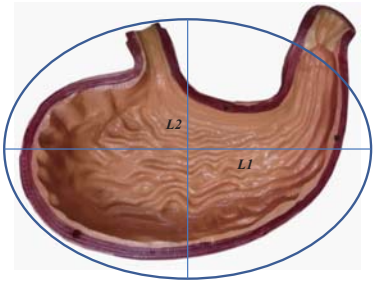

Fig. 11. 1:1 human stomach model and spatial scale. L1=230mm, L2=130mm. An ellipse is used to approximate the actual workspace.

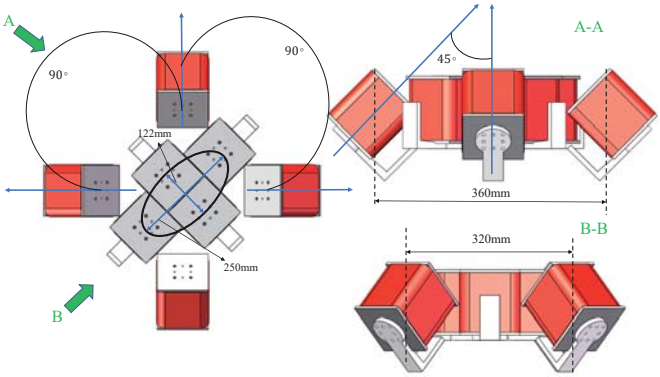

Fig. 12. Magnetic manipulation system conceptual design framework and physical parameters of spatial arrangement.

III. EXPERIMENTAL ASSESSMENT

A. Magnetic Field Distribution

When the spatial configuration of the magnetic field module is determined, we need to master the magnetic field distribution to apply torque and force to the magnetic capsule robot remotely. Our previous work modeled the magnetic field mathematical model based on the Biot-Savart law for single-layer coils and verified the accuracy of the magnetic field distribution and the real-time performance of the system [17], [18]. As shown in Fig.15, we extended to multi-layer

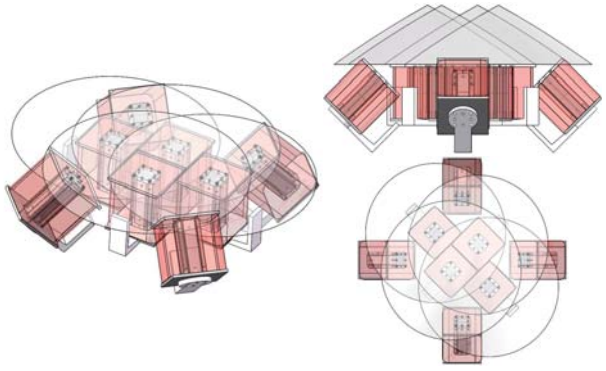

Fig. 13. Main coil module crosses superimposed magnetic field radiation area.

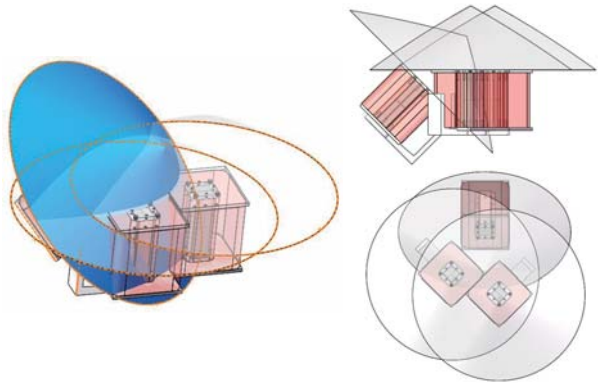

Fig. 14. Auxiliary coil module crosses superimposed magnetic field radiation area.

coils to comply with the electromagnetic coil module structure proposed in the section II(a), the length, width and height of the first layer of this rectangular coil are $2l$, $2w$ and $2h$ respectively. The magnetic field at the position P=(a,b,c) can be calculated as follows:

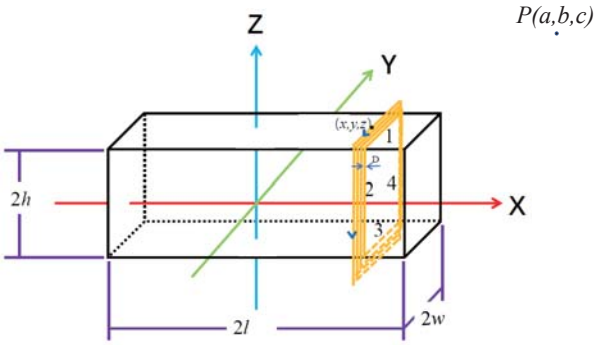

Fig. 15. Modelling of the multi-layer rectangular coil. The coordinate system is based on the coil. The X-axis is along with the length of the coil and the origin of the coordinate is at the center position of the coil. The direction of the current I is different in the four different planes.

$$y_1 = y+nD; z_1 = z+nD; w_1 = w+nD; h_1 = h+nD; K_r = J_s\mu_0$$

where D is the diameter of the coil, J_s is the current density(A/m). For segment 1:

$$\begin{cases} dB_{x1} = \sum_{n=0}^{N-1} K_r dx \int_{-w_1}^{w_1} \frac{-(c-h_1)}{((a-x)^2+(b-y_1)^2+(c-h_1)^2)^{\frac{3}{2}}} dy_1 \\ dB_{y1} = 0 \\ dB_{z1} = \sum_{n=0}^{N-1} K_r dx \int_{-w_1}^{w_1} \frac{a-x}{((a-x)^2+(b-y_1)^2+(c-h_1)^2)^{\frac{3}{2}}} dy_1 \end{cases}$$

For segment 2:

$$\begin{cases} dB_{x2} = \sum_{n=0}^{N-1} K_r dx \int_{-h_1}^{h_1} \frac{b+w_1}{((a-x)^2+(b+w_1)^2+(c-z_1)^2)^{\frac{3}{2}}} dy_1 \\ dB_{y2} = \sum_{n=0}^{N-1} K_r dx \int_{-h_1}^{h_1} \frac{-(a-x)}{((a-x)^2+(b+w_1)^2+(c-z_1)^2)^{\frac{3}{2}}} dy_1 \\ dB_{z2} = 0 \end{cases}$$

For segment 3:

$$\begin{cases} dB_{x3} = \sum_{n=0}^{N-1} K_r dx \int_{-w_1}^{w_1} \frac{c+h_1}{((a-x)^2+(b-y_1)^2+(c+h_1)^2)^{\frac{3}{2}}} dy_1 \\ dB_{y3} = 0 \\ dB_{z3} = \sum_{n=0}^{N-1} K_r dx \int_{-w_1}^{w_1} \frac{-(a-x)}{((a-x)^2+(b-y_1)^2+(c+h_1)^2)^{\frac{3}{2}}} dy_1 \end{cases}$$

For segment 4:

$$\begin{cases} dB_{x4} = \sum_{n=0}^{N-1} K_r dx \int_{-h_1}^{h_1} \frac{-(b-w_1)}{((a-x)^2+(b-w_1)^2+(c-z_1)^2)^{\frac{3}{2}}} dy_1 \\ dB_{y4} = \sum_{n=0}^{N-1} K_r dx \int_{-h_1}^{h_1} \frac{a-x}{((a-x)^2+(b-w_1)^2+(c-z_1)^2)^{\frac{3}{2}}} dy_1 \\ dB_{z4} = 0 \end{cases}$$

$$\begin{aligned} B_{rx} = \sum_{n=0}^{N-1} (K_r (& f_{r1}(a, c-h_1, b-w_1) - f_{r1}(a, c-h_1, b+w_1) \\ & + f_{r1}(a, b+w_1, c+h_1) - f_{r1}(a, b+w_1, c-h_1) \\ & + f_{r1}(a, c+h_1, b+w_1) - f_{r1}(a, c+h_1, b-w_1) \\ & + f_{r1}(a, b-w_1, c-h_1) - f_{r1}(a, b-w_1, c+h_1))) \end{aligned} \tag{1}$$

$$\begin{aligned} B_{ry} = \sum_{n=0}^{N-1} (K_r (& f_{r2}(a, b+w_1, c-h_1) - f_{r2}(a, b+w_1, c+h_1) \\ & + f_{r2}(a, b-w_1, c+h_1) - f_{r2}(a, b-w_1, c-h_1))) \end{aligned} \tag{2}$$

$$\begin{aligned} B_{rz} = \sum_{n=0}^{N-1} (K_r (& f_{r2}(a, c-h_1, b+w_1) - f_{r2}(a, c-h_1, b-w_1) \\ & + f_{r2}(a, c+h_1, b-w_1) - f_{r2}(a, c+h_1, b+w_1))) \end{aligned} \tag{3}$$

where

$$\begin{aligned} f_{r1}(a,b,c) = & -atan\left(\frac{c(a-l)}{b\sqrt{((a-l)^2+b^2+c^2)}}\right) \\ & + atan\left(\frac{c(a+l)}{b\sqrt{((a+l)^2+b^2+c^2)}}\right) \end{aligned} \tag{4}$$

$$\begin{aligned} f_{r2}(a,b,c) = & atanh\left(\frac{\sqrt{((a-l)^2+b^2+c^2)}}{c}\right) \\ & - atanh\left(\frac{\sqrt{((a+l)^2+b^2+c^2)}}{c}\right) \end{aligned} \tag{5}$$

The force can be obtained by the equations as follows:

$$F = \begin{bmatrix} \frac{\partial B_{rx}}{\partial x} & \frac{\partial B_{rx}}{\partial y} & \frac{\partial B_{rx}}{\partial z} \\ \frac{\partial B_{ry}}{\partial x} & \frac{\partial B_{ry}}{\partial y} & \frac{\partial B_{ry}}{\partial z} \\ \frac{\partial B_{rz}}{\partial x} & \frac{\partial B_{rz}}{\partial y} & \frac{\partial B_{rz}}{\partial z} \end{bmatrix} M$$

Input current vector to force and torque control mapping equation can be written as follows:

$$\begin{pmatrix} T \\ F \end{pmatrix} = \begin{pmatrix} S_k(M)\beta \\ M^T\beta_x \\ M^T\beta_y \\ M^T\beta_z \end{pmatrix} \begin{pmatrix} i_1 \\ \vdots \\ i_8 \end{pmatrix} = A_{T,F}(M)I \tag{6}$$

However, in this paper, the magnetic field distribution we constructed does not take into account the coupling relationship between the magnetic field modules, because we only test whether the platform has the basic ability to actuate the magnetic capsule robot and accurate control of position and orientation will be carried out in the future.

B. Experimental Process and Results

The magnetic capsule robot preset trajectory is first discretized into scatter points in space, and the desired force and torque at these points are then determined. Finally, the discrete current sequence is obtained by using equation (6). As shown in Fig.16 and Fig.17, open-loop experiments were carried out to verify the system's ability to implement the basic functions of controlling magnetic capsule robots.

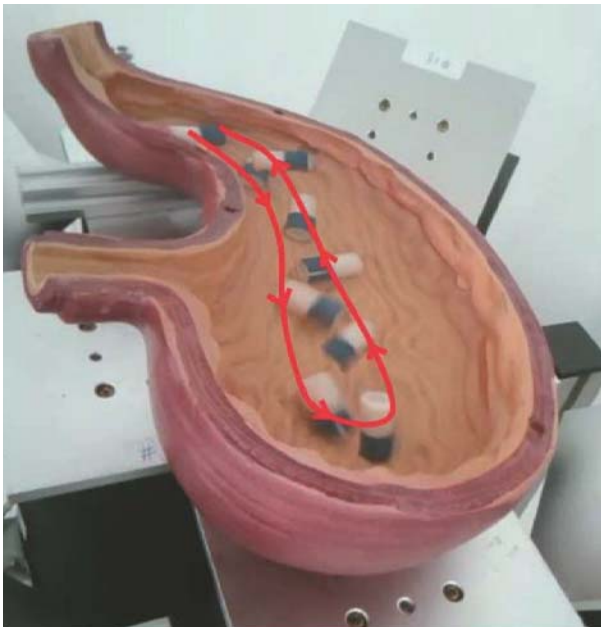

Fig. 16. Spatial position control experiment of magnetic capsule robot in stomach model.

IV. CONCLUSIONS

In this paper, we designed a novel open electromagnetic actuation system for a specific medical application for gastrointestinal magnetic capsule endoscopy. Utilizing finite element analysis to optimize the physical parameters of the coil module and realize the visual characterization design of the effective radiation area of the magnetic field can effectively compensate for the small effective working area of the electromagnetic operating system comparing with the permanent magnet actuation system. Although the electromagnetic actuation system can not simultaneously control the 3-DOF position and 2-DOF orientation of the magnetic capsule robot, the experimental results in this paper demonstrate its functional realization in the medical application of magnetic capsule endoscopy. In addition, its expandable properties demonstrate its potential. In the future, the following work will be carried

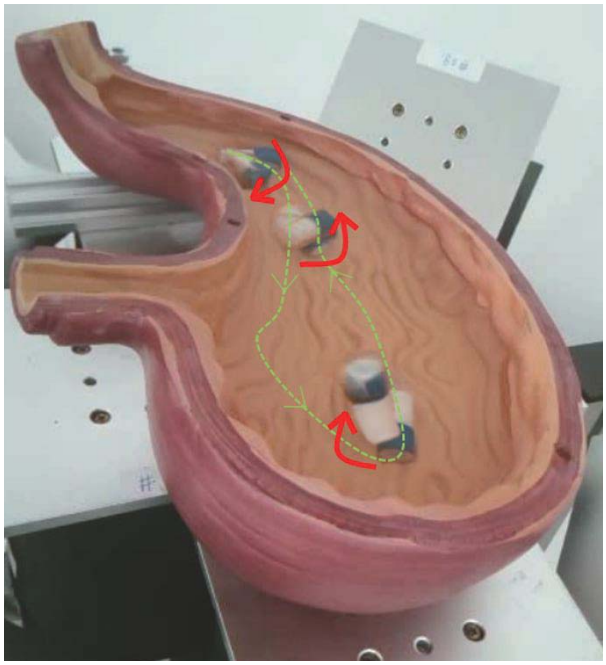

Fig. 17. The magnetic capsule robot realizes rotation at the planned position.

out: Firstly, an accurate mathematical model of the magnetic field distribution of the electromagnetic actuation system will be studied. We want to utilize a more concise expression to characterize the coupled magnetic field and the gradient of the field. Secondly, this system will be combined with the magnetic positioning system and optical positioning system to achieve accurate trajectory planning and image transmission of the magnetic capsule robot in the body. Finally, we will optimize the selection decision of the input current sequence to reduce the heat generation and extended working time of the system.

REFERENCES

[1] Reavis, K. M., & Melvin, W. S. (2008). Advanced endoscopic technologies. Surgical Endoscopy, 22(6), 1533-1546.

[2] Moglia, A., Menciassi, A., Schurr, M. O., & Dario, P. (2007). Wireless capsule endoscopy: from diagnostic devices to multipurpose robotic systems. Biomedical microdevices, 9(2), 235-243.

[3] Westerhof, J., Weersma, R. K., & Koornstra, J. J. (2009). Risk factors for incomplete small-bowel capsule endoscopy. Gastrointestinal endoscopy, 69(1), 74-80.

[4] Ciuti, G., Menciassi, A., & Dario, P. (2011). Capsule endoscopy: from current achievements to open challenges. IEEE reviews in biomedical engineering, 4, 59-72.

[5] Rahmer, J., Stehning, C., & Gleich, B. (2018). Remote magnetic actuation using a clinical scale system. PloS one, 13(3), e0193546.

[6] Nelson, B. J., Kaliakatsos, I. K., & Abbott, J. J. (2010). Microrobots for minimally invasive medicine. Annual review of biomedical engineering, 12, 55-85.

[7] Mahoney, A. W., & Abbott, J. J. (2016). Five-degree-of-freedom manipulation of an untethered magnetic device in fluid using a single permanent magnet with application in stomach capsule endoscopy. The International Journal of Robotics Research, 35(1-3), 129-147.

[8] Yesin, K. B., Vollmers, K., & Nelson, B. J. (2006). Modeling and control of untethered biomicrorobots in a fluidic environment using electromagnetic fields. The International Journal of Robotics Research, 25(5-6), 527-536.

[9] Jeon, S. M., Jang, G. H., Choi, H. C., Park, S. H., & Park, J. O. (2011). Utilization of magnetic gradients in a magnetic navigation system for the translational motion of a micro-robot in human blood vessels. IEEE Transactions on Magnetics, 47(10), 2403-2406.

[10] Yu, C., Kim, J., Choi, H., Choi, J., Jeong, S., Cha, K., ... & Park, S. (2010). Novel electromagnetic actuation system for three-dimensional locomotion and drilling of intravascular microrobot. Sensors and Actuators A: Physical, 161(1-2), 297-304.

[11] Kummer, M. P., Abbott, J. J., Kratochvil, B. E., Borer, R., Sengul, A., & Nelson, B. J. (2010). OctoMag: An electromagnetic system for 5-DOF wireless micromanipulation. IEEE Transactions on Robotics, 26(6), 1006-1017.

[12] Petruska, A. J., Brink, J. B., & Abbott, J. J. (2015, May). First demonstration of a modular and reconfigurable magnetic-manipulation system. In 2015 IEEE International Conference on Robotics and Automation (ICRA) (pp. 149-155). IEEE.

[13] Son, D., Dogan, M. D., & Sitti, M. (2017, May). Magnetically actuated soft capsule endoscope for fine-needle aspiration biopsy. In 2017 IEEE International Conference on Robotics and Automation (ICRA) (pp. 1132-1139). IEEE.

[14] Son, D., Dong, X., & Sitti, M. (2018). A Simultaneous Calibration Method for Magnetic Robot Localization and Actuation Systems. IEEE Transactions on Robotics, 35(2), 343-352.

[15] Erni, S., Schrle, S., Fakhraee, A., Kratochvil, B. E., & Nelson, B. J. (2013). Comparison, optimization, and limitations of magnetic manipulation systems. Journal of Micro-Bio Robotics, 8(3-4), 107-120.

[16] Petruska, A. J., & Nelson, B. J. (2015). Minimum bounds on the number of electromagnets required for remote magnetic manipulation. IEEE Transactions on Robotics, 31(3), 714-722.

[17] Shuang S, Haoyong Y, Hongliang R. Study on Mathematic Magnetic Field Model of Rectangular Coils for Magnetic Actuation[C]//Proceeding of the IEEE International Conference on Robotics and Biomimetics, 2015: 19-24.

[18] Hao G, Shuang S, Max M. RectMag: A Accurate Magnetic Field Model Based Actuation System[C]// Proceeding of the IEEE International Conference on Robotics and Biomimetics, 2016: 23-28.